Carbohydrate Polymers 345 (2024) 122591

Contents lists available at ScienceDirect

Carbohydrate Polymers

journal homepage: www.elsevier.com/locate/carbpol

Modulating the isotopic hydrogen-deuterium exchange in functionalized nanocellulose to optimize SANS contrast

Vikram Singh Raghuwanshi [a,*], David Joram Mendoza [b], Jitendra Mata [c,d], Gil Garnier [a,*]

[a] Bioresource Processing Research Institute of Australia (BioPRIA), Department of Chemical and Biological Engineering, Monash University, Clayton, Victoria 3800, Australia
[b] Department of Materials Science and Engineering, Monash University, Clayton, Victoria 3800 Australia
[c] Australian Centre for Neutron Scattering (ACNS), Australian Nuclear Science and Technology Organisation (ANSTO), Lucas Height, New South Wales 2234, Australia
[d] School of Chemistry, University of New South Wales, NSW, Australia

ARTICLE INFO

Keywords:
Contrast matching
Nanocellulose
Small angle neutron scattering (SANS)
H_2O
D_2O
Deuterium
Isotope
poly-N-isopropylacrylamide (PNIPAM)
Cellulose nanofibers (CNF)
Cellulose nanocrystals (CNC)
Microcrystalline cellulose (MCC)
ATR-FTIR

ABSTRACT

Contrast matching by isotopic exchange in cellulose allows visualizing functional groups, biomolecules, polymers and nanoparticles embedded in cellulosic composites. This isotopic exchange varies the scattering length density of cellulose to match its contrast with the background network.

Here, contrast matching of microcrystalline-cellulose (MCC) and the functionalized nanocellulose-fiber (CNF) and cellulose nanocrystals (CNC) are elucidated by small angle neutron scattering (SANS). Results show no isotopic exchange occurs for the CNF surface functionalized with carboxyl nor for the CNC-**High** with a high sulfate groups concentration.

Both CNC-**Low**, with low sulfate groups, and MCC exchange 1H with 1D in D_2O. This is due to the high exchange probability of the labile C_6 position primary -OH group.

The structure of thermo-responsive poly-N-isopropylacrylamide (PNIPAM) chains grafted onto CNF (PNIPAM-grafted-CNF) was extracted by CNF contrast matching near the lower critical solution temperature. Contrast matching eradicates the CNF scattering to retain only the scattering from the grafted-PNIPAM chains. The coil to globule thermo-transition of PNIPAM was revealed by the power law variation from $q^{-1.3}$ to q^{-4} in SANS.

Isotopic exchange in functionalized cellulosic materials reveals the nano- and micro-scale structure of its individual components. This improved visualization by contrast matching can be extended to carbohydrate polymers to engineer biopharmaceutical and food applications.

1. Introduction

Cellulosic micro- and nano-materials are thoroughly used for developing sustainable and functional materials with emerging applications such as biopharmaceutical, food and photonics (Li et al., 2021; Müller et al., 2022). Chemically, cellulose is a biopolymer made of hydrogen, carbon and oxygen atoms polymerized into linear chains of anhydroglucose bonded with the β-1,4-glycosidic bond so the C_1 of one monomer links with the C_4 of another inverted unit (Penttilä et al., 2021; Wohlert et al., 2022). There are three -OH groups present at C_2, C_3 and C_6 positions of the monomer. The primary -OH linked to the C_6 carbon has a higher probability to exchange and functionalize than the secondary -OH groups at the C_2 and C_3 position. The hydroxyl group at the C_6 is also responsible for the strong hydrogen (H) binding among chains, conferring nanocellulose its rigidity and compactness. The linear chains of cellulose organize in an alternative crystalline and amorphous phase to become the building blocks of plants and trees.

Exchanging hydroxyl groups from the cellulose monomeric unit with functional groups creates new material with unique properties that can be tailored for a wide range of applications. Among those processes, the TEMPO-mediated (2,2,6,6-tetramethylpiperidine-1-oxyl) oxidation incorporates carboxyl groups on nanocellulose fiber (CNF) monomer unit (Saito & Isogai, 2004).

The CNF extracted with the TEMPO process has a high COOH surface concentration yielding a high negative charge density which contributes to forming stable hydrogels and transparent films for biomedical (Curvello, Raghuwanshi, & Garnier, 2019), cosmetics, electronics (Xu et al., 2021), packaging (Amoroso et al., 2022), and food (Perumal, Nambiar,

* Corresponding authors.
E-mail addresses: vikram.raghuwanshi@monash.edu (V.S. Raghuwanshi), gil.garnier@monash.edu (G. Garnier).

https://doi.org/10.1016/j.carbpol.2024.122591
Received 4 April 2024; Received in revised form 1 August 2024; Accepted 6 August 2024
Available online 8 August 2024

Moses, & Anandharamakrishnan, 2022) applications. Cellulose nanocrystals (CNC) extracted by sulfuric acid hydrolysis are embedded with negative sulfate groups (George & Sabapathi, 2015). Additional post hydrolysis reactions can introduce aldehyde, amino or thiol groups on the CNC surface (Tang, Sisler, Grishkewich, & Tam, 2017). These rod-shaped CNCs self-assemble in a chiral nematic helix which makes them attractive materials for applications in photonics (Raghuwanshi, Vir, Lin, & Garnier, 2023), electronics, sensors (Bethke et al., 2018) and catalysis.

The different properties and applications of functional nanoscale cellulose (CNF and CNC) composites rely on the distribution and interactions of the individual entities within the composite. It is still very challenging to extract accurate structural information due to the nanoscale dimensions, the interactions, sample preparation artefacts and the poor visualizing contrast between entities. Only a few characterization methods, such as scanning and transmission electron microscopy (SEM/TEM), Atomic Force Microscopy and small angle X-ray and neutron scattering (SAXS/SANS), can provide reliable nanoscale information (1–500 nm). While electron microscopy offers real space imaging, it requires complex sample preparation and can only be performed in a dried state. Sample preparation often creates artefacts and further, poor electron density difference between CNF and other entities makes it difficult to visualize and resolve distributions.

SAXS and SANS are non-destructive methods that determine the nanoscale structural properties and interactions directly in the as prepared sample state (Feigin, 1987; Glatter, 1982; Raghuwanshi & Garnier, 2019). SAXS is however limited by the low electron density of biopolymers, radiation damage and poor scattering contrast variation. In that respect, low energy SANS emerges as a compelling method to characterize the nanoscale structure of biopolymers. Further, SANS exploits the large scattering length density (SLD) difference between hydrogen (H) and its isotope deuterium (D) to modulate the scattering contrast of the various individual entities.

Exchanging H with D in cellulosic systems provides the required contrast to reveal the shape, size, distribution and interaction of fibers or to only focus on the specific functionalities of interest in a network. Paavo et al. monitored the water diffusion and interactions in the plant cell walls by SANS[3]. Deuteration of cellulose elucidated the dissolution mechanisms of cellulose in ionic liquids (Raghuwanshi et al., 2018; Raghuwanshi, Cohen, Garnier, Garvey, & Garnier, 2021) and improved visualizing bio-molecules adsorption over thin film interfaces (Cheng et al., 2011; Huang, Raghuwanshi, & Garnier, 2017; Su et al., 2016).

The three labile H are available on the cellulose unit cell for isotopic exchange allows matching the scattering contrast of cellulose and visualizing other molecular or chemical entities of interest in cellulosic composites (Martínez-Sanz, Gidley, & Gilbert, 2016; Song et al., 2022). The contrast matches at the minimum SLD difference between the cellulose and dispersed H_2O/D_2O suspension. Previous literature reported the H_2O/D_2O ratio of 65/35 to be the matching point for cellulose (Crawshaw, Vickers, Briggs, Heenan, & Cameron, 2000; Penttilä et al., 2021). This ratio considers no exchange of H with D between solvent and the cellulose unit in suspension. However, it is plausible and even probable that D atoms from the solvent can replace H atoms at the C_6 position of the cellulosic unit. Such H/D exchange in the emerging functionalized nanocellulose (CNF and CNC) is even more critical as the C_6 position is already occupied by a functional group (-COOH and $-SO_4^-$, respectively). Thus, it is important to understand and control this H/D exchange phenomenon in the emerging functionalized celluloses in H_2O/D_2O suspension; this is to engineer the contrast matching and reveal the water molecules interaction at the nanoscale of cellulose units. This enables optimum visualization of the nanostructure of these complex carbohydrate polymers and the ability to only focus on the functionality of interest.

This study aims to determine the selectivity and impact of exchanging -OH groups with -OD groups in the nanoscale characterization of functionalized CNF and CNC. SANS and FTIR experiments are performed using three different types of nano/micro cellulose dispersed in H_2O/D_2O as suspensions: pure microcrystalline cellulose (MCC), sulfate functionalized cellulose nanocrystals (CNC) and carboxyl functionalized TEMPO-oxidized cellulose nanofibers (CNF). Results reveal the difference in the isotopic level exchange of H to D for functionalized cellulose compared to the pure cellulose. Finally, as proof of concept, thermosensitive poly(N-isopropylacrylamide) (PNIPAM)-grafted-CNF is studied to demonstrate the benefits of matching the CNF contrast to visualize the grafted PNIPAM corona distribution in hydrogels that is otherwise undistinguishable.

2. Experiments

2.1. Materials

Two different types of commercial cellulose nanocrystals (CNC) were purchased from CelluForce, Pointe Claire, Canada (CNC-**Low**) and the Process Development Centre, University of Maine, USA (CNC-**High**), respectively. The CNC-**Low** is in the powder form which is dispersed into 1 wt% suspensions at different ratio of H_2O/D_2O varying from 0 to 100. CNC-**High** is received in a gel form with a solid concentration of 10.3 wt % and was diluted to 1 wt% into different H_2O/D_2O suspensions. Both CNC-**Low** and CNC-**High** contain the sulfate groups. The CNC-**Low** contains less sulfate groups (0.53 % S elemental sulfur content) compared to the CNC-**High** (0.73 %) (Browne, Raghuwanshi, Lin, Garnier, & Batchelor, 2022; Raghuwanshi, Browne, Batchelor, & Garnier, 2023). The TEMPO-oxidized cellulose nanofibers (CNF) with a carboxylate content of 1.4 mmol COO^-Na^+/g were purchased from the University of Maine, USA. The CNF was received as a gel form with a solid concentration of 1.27 wt%. The CNF was diluted to 0.1 wt% into suspensions at different H/D ratios (vol%). Microcrystalline cellulose (MCC) in the powder form was purchased from Sigma Aldrich. The MCC pastes were processed into suspensions (1 g MCC in 5 mL water) at different H/D ratios (vol%). The PNIPAM-grafted-CNF samples were prepared from the method published previously (Mendoza et al., 2022; Raghuwanshi et al., 2023).

2.2. Fourier Transform Infra-red spectroscopy (FTIR)

Attenuated total reflectance (ATR)-FTIR was conducted on the air dried samples of CNC-**High**, CNC-**Low**, MCC and CNF. The samples were prepared in D_2O and air dried overnight at lab room temperature. The ATR-FITR measurements were conducted using an Agilent Technologies Cary 630 FTIR spectrometer. The spectra were collected in the range of 4000–500 cm^{-1}. In the post treatment, the raw data was subtracted by the baseline and normalized using the OriginPro software.

2.3. Small-angle neutron scattering (SANS)

Small-angle neutron scattering (SANS) measurements were performed at the Quokka beamline at the Australian Nuclear Science and Technology Organisation (ANSTO), Australia (Wood et al., 2018). Demountable cells of different thickness 1 mm and 2 mm equipped with quartz window were used. For the suspensions with H_2O concentration equal and higher than 50 %, the 1 mm thick cell was selected; the 2 mm thick cell was used for suspensions with H_2O concentration lower than 50 %. Samples were made in different H_2O/D_2O ratio suspensions and were filled in the cells and measured in the transmission mode at two different detector distances: 2 m and 12 m with a wavelength was 5 Å. Scattering from blocked beam, Empty cell, D_2O and H_2O filled cell were also measured to correct the background scattering. Suspensions of different H_2O/D_2O ratios were also measured with the sample as background which was subtracted from the individual sample prepared at that particular H_2O/D_2O ratio. The raw scattering data was reduced and normalized to the absolute scattering cross section using the home-built Quokka data reduction package with the Igor software (Kline, 2006).

Further data analysis was performed by fitting the reduced SANS curve by shape form factor of the long cylinder core shell model using the SASfit software (Breßler, Kohlbrecher, & Thünemann, 2015).

3. Results

3.1. Cellulose nanocrystals

Two samples of cellulose nanocrystals (CNC) varying in sulfonate concentration were tested. Previous structural characterization of both CNCs reveals the diameter to be of 3–5 nm and length between 100 and 150 nm (Raghuwanshi, Browne, et al., 2023). The number of anhydroglucose units (AGU) available on a CNC surface is about 3885, as evaluated from the two dimensions of an AGU cell: a = 0.61 nm and b = 0.54 nm (Okita, Saito, & Isogai, 2010; Wada, Okano, & Sugiyama, 1997) (SI.1). During CNC production, only the surface is exposed to the functionalisation and isotopic exchange, while the inner core remains as pure cellulose. CNC-**High** has a high elemental sulfur content (%S) concentration of 0.73 % ± 0.09, while it is 0.57 % ± 0.06 for the lower CNC-**Low**. The sulfate half-ester content (mmol/g) for CNC-**High** and CNC-**Low** were 0.23 % ± 0.03 and 0.18 % ± 0.02. As the sulfonate substitutes the OH on C_6, a higher content reduces the availability of labile -OH groups able to undergo reversible exchange D/H. The sulfonate group density also contributes to charge stabilizing CNC in suspensions.

3.2. CNC-*High*

Fig. 1a shows the CNC-**High** suspensions SANS curves measured at different H_2O/D_2O ratios. Since the CNC-**High** was available as a 10 wt % consistency gel, the effective H_2O/D_2O ratio achievable ranges from 10/90 to 100/0. The intensity of the SANS curve decreases as increases the H_2O/D_2O ratio until the inflection ratio of 60/40 (Fig. 1a) is reached, from which intensity starts again to increase with the H/D solvent ratio (Fig. 1b). This minimum in scattering intensity reveals the contrast matching point where the scattering length density (SLD) of the CNC-**High** matches that of the solvent, here H_2O/D_2O at the 60/40 ratio.

The scattering curves fit well with the form factor of a long cylinder core-shell combined with a lognormal distribution. Only the surface of the CNC is functionalized with the sulfate groups and exposed for isotopic exchange. Thus, we have assumed the cylindrical core shell model. In this model, the core is pure cellulose and the shell consists of cellulose

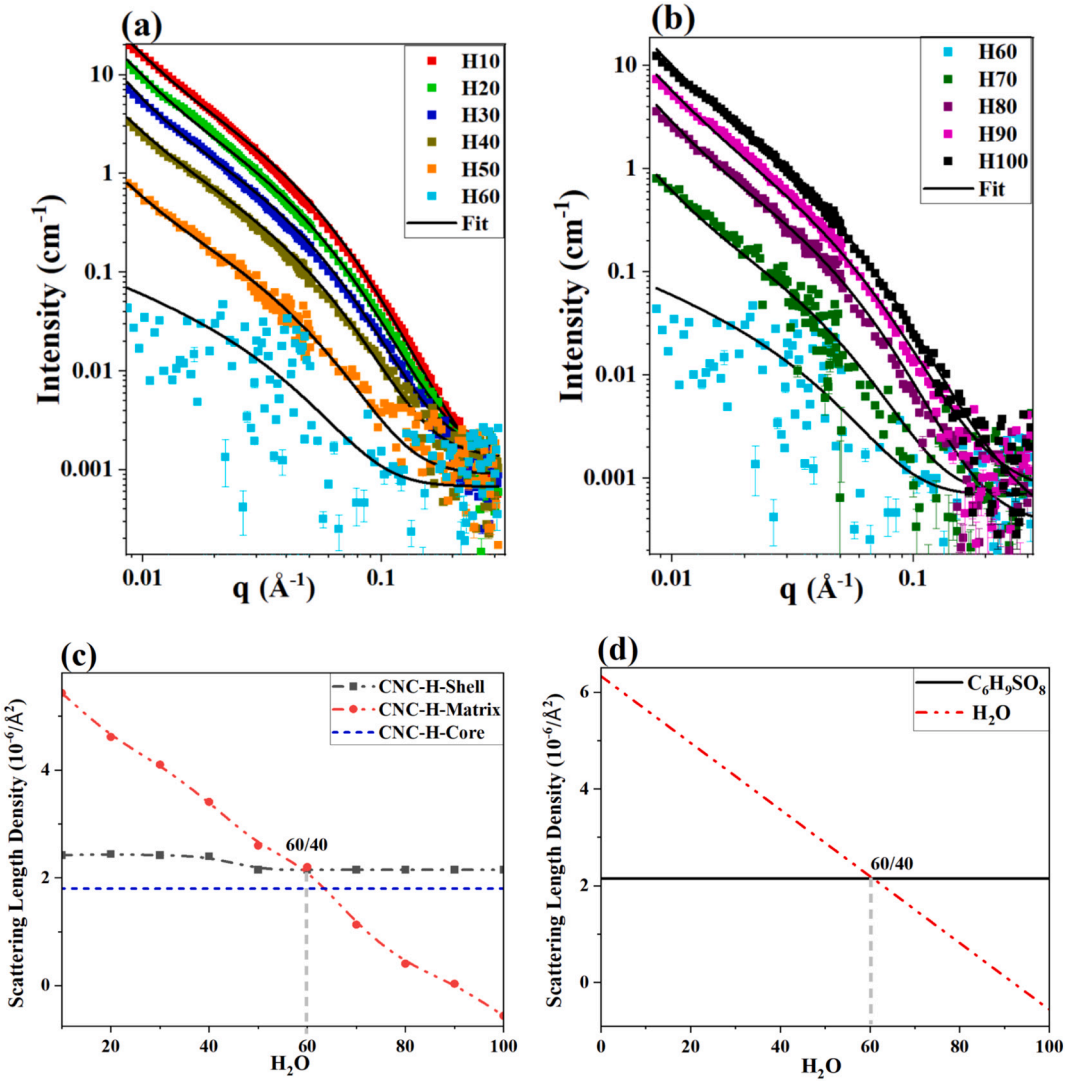

Fig. 1. (a) Intensity- q vector SANS curves from nanocellulose crystal (CNC-**High**) suspensions measured in H_2O/D_2O at ratios of: (a) H10 to H60 (wt%) and (b) H60 to H100 (wt%). (c) Experimental SLD variation profile of core (pure cellulose), shell and matrix are plotted against the H_2O concentration. The contrast matching point for shell and matrix is at 60/40 (d) Theoretical SLD of CNC-**High** plotted against the H_2O concentration. The cross section at H_2O/D_2O ratio 60/40 is the contrast matching point.

units with a sulfate group exchanged at the C_6 position. The SLDs of the core and shell are provided in Table 1. For calculating SLD for CNF, a mass density of 1.6 g/cm^3 is used (Yano et al., 2018). The density of crystalline cellulose is reported to be between 1.5 and 1.6 g/cm^3 (Mariano, El Kissi, & Dufresne, 2014). Thus, an average of 1.55 g/cm^3 is used for calculating the SLD of MCC and CNC. Details of the cylindrical core shell model are provided in the supporting information (SI.2). Fitting parameters reveals the CNC diameter to range between 3 and 5 nm, the length to be 100–150 nm and the shell about 0.5 nm thick. In the multiple curves fitting performed, all structural parameters are kept constant only to vary the scattering contrast of shell and solvent. The evaluated SLD of shell and matrix from fitting is plotted against the H_2O/D_2O ratio (Fig. 1c). The cross-section of shell and matrix reveals the contrast matching point at the H_2O/D_2O ratio of 60 ± 1.0. The theoretical SLD calculated for CNC with sulfate group plot against H_2O variation shows the contrast matching at a H_2O/D_2O ratio of 60/40 (Fig. 1d).

The CNC-**High** SLD calculated from the cellulose monomeric unit having one sulfate (SO_4^-) group ($C_6H_9SO_8^-$) substituted on the C_6 carbon is 2.15 × 10^{-6} (Å^{-2}). A sulfate group from the sulfuric acid used in the cellulose nanocrystals process replaces the hydrogen atom of cellulose at the C_6 position. The theoretical and the experimental match point in Fig. 1c and d are similar with a minimum at the H_2O/D_2O ratio of 60/40. This analysis reveals that no exchange H—D occurred for CNC-**High**.

3.3. CNC-*Low*

Fig. 2 shows the SANS curves of CNC-**Low** suspensions equilibrated and measured at different H_2O/D_2O ratios. The CNC-**Low** was in the powder form so the full H_2O/D_2O ratio ranging from 0/100 to 100/0 is achievable. Similar to CNC-**High**, CNC-**Low** also shows a parabolic relationship with first a decrease in the scattering intensity as increases the H_2O/D_2O ratio until the minimum is reached at a ratio of 60/40 (Fig. 2a). Further increases in the H_2O/D_2O ratio starts increasing the scattering intensity (Fig. 2b).

The scattering curves were also fitted similarly with the long cylinder core-shell model and the extracted SLD is plotted in Fig. 2c. The SLD of the shell and matrix model evaluated from fitting is plotted against the H2O/D2O ratio (Fig. 2c). The cross-section of shell and matrix reveals the contrast matching point at the H_2O/D_2O ratio of 60 ± 1.0. The calculated SLD of CNC-**Low** (2.15 × 10^{-6} Å^{-2}) with a mass density of 1.55 g/cm^3 is assumed to be similar to that of CNC-**High** as both are calculated from cellulose monomers with a low substitution of sulfate (SO_4^-) groups ($C_6H_9SO_8$). Further, the contrast matching points of both CNC-**Low** and -**H**igh are similar.

Table 1
Chemical formula, scattering length density (SLD) and functional group on the nanocellulose fiber (CNF) and cellulose nanocrystals (CNC). The CNC-**High** and CNC-**Low** have different functional sulphate group amounts but a similar chemical formula is considered. The microcrystalline-cellulose (MCC) is pure cellulose without any functional group.

Cellulose	Chemical formula core	SLD core ×10^{-6} Å^{-2}	Chemical formula shell	SLD shell ×10^{-6} Å^{-2}	Functional group in shell
Cellulose nanocrystals (CNC)	$C_6H_{10}O_5$	1.8	$C_6H_9SO_8^-$	2.15	$-SO_4^-$
Cellulose nanofibers (CNF)	$C_6H_{10}O_5$	1.8	$C_6H_7O_6^-$	2.67	$-COO^-$
Microcrystalline cellulose (MCC)	$C_6H_{10}O_5$	1.8	–	–	–

3.4. Cellulose nanofibers (CNF)

Cellulose nanofibers (CNF) are typically made by TEMPO-oxidation followed by homogenization. This produces defibrillated nanofibrils with the C_6 primary hydroxyl typically substituted by a carbonyl (COOH). SANS curves of the cellulose nanofiber (CNF) suspensions were measured at different H_2O/D_2O solvent ratios (Fig. 3a). As the original CNF was provides as a gel with a solid content of 1.27 wt%, the H_2O/D_2O ratio achievable ranges from 10/90 to 90/10. Similar to the CNC-**Low** and CNC-**High**, CNF suspensions show first a decrease in the scattering intensity with the minimum scattering intensity observed at 50/50 H_2O/D_2O ratio. Any further increase in H_2O/D_2O ratio increases the scattering intensity. By the fitting scattering curves with a long cylinder core-shell model, the extracted SLD of core, shell and matrix is plotted against the H_2O content (Fig. 3b). The cross section of shell and matrix reveals the contrast matching point is at the H_2O/D_2O ratio of 52/48.

Theoretically, the SLD of CNF is calculated from a cellulose monomer unit with one carboxyl (COO^-) group at the C_6 position ($C_6H_7O_6$). During the TEMPO oxidation, the COO^- groups replace the primary -OH at the C_6 position. We expect and assume all -OH groups at the C_6 position of the CNF chain monomer to be substituted by COO^- groups. The SLD calculated for CNF is 2.67 × 10^{-6} Å^2 assuming a mass density of 1.6 g/cm^3. The SLD plot of CNF with change in H_2O concentration reveals the contrast matching point at the cross-section of H_2O/D_2O ratio of 52/48 (Fig. 3c). The experimental contrast value is at a H_2O/D_2O ratio of 52/48 which matches the theoretical value of 52/48 (Fig. 3b). This result indicates that in D_2O at room temperature, none of the secondary -OH groups at the C_2 and C_3 position of cellulose are exchanged by -OD groups.

3.5. Microcrystalline cellulose (MCC)

The CNC-**Low**, CNC-**High** and TEMPO-oxidized CNF discussed above were functionalized with the sulfate and carboxyl group, respectively, which also stabilizes the suspension and forms gels. However, the microcrystalline cellulose (MCC) is processed from cotton linters and is pure cellulose -without any functional groups. The chemical formula of the MCC monomer is $C_6H_{10}O_5$ with the primary -OH group present at the C_6 position and two other secondary hydroxyls at the position of C_2 and C_3.

The SANS experiments were performed from the MCC powder suspended at different ratio of H_2O/D_2O. Since the MCC was received as a powder, the full H_2O/D_2O ratio ranging from 0/100 to 100/0 was used. The SANS intensity decreases as increases the H_2O/D_2O ratio until 60/40 (Fig. 4b) to then further increase with H/D ratio (Fig. 4b). Thus, the minimum of the scattering intensity is expected to be near the H_2O/D_2O ratio of 60/40. The MCC curves fit well with the long cylinder-shell model and the extracted SLD of core, shell and matrix is plotted in Fig. 4c. For the shell SLD no exchange of H with D is considered at the H_2O/D_2O ratio higher than 65/35. The contrast match point at the cross section of the shell and matrix is at the H_2O/D_2O ratio of 58/42.

The theoretical SLD of the MCC ($C_6H_{10}O_5$) is 1.8 × 10^{-6} (Å^{-2}) for no exchange of -OH groups and density of 1.55 g/cm^3. The scattering contrast match point at the cross-section without any exchange is calculated at the H_2O/D_2O ratio of 65/35 (Fig. 4d). The SLD value increased to 2.4 × 10^{-6} (Å^{-2}) as one -OH group exchanges for one -OD group ($C_6D_1H_9O_5$). The theoretical scattering contrast match point is comparable to the experimental shell-matrix at 58/42 H_2O/D_2O ratio (Fig. 4c). The contrast matching point is also shown at the cross-section in Fig. 4d. Comparing the theoretical and experimental contrast indicates that one of the -OH group from MCC is replaced with one -OD groups in D_2O; this is expected to occur at the C_6 position.

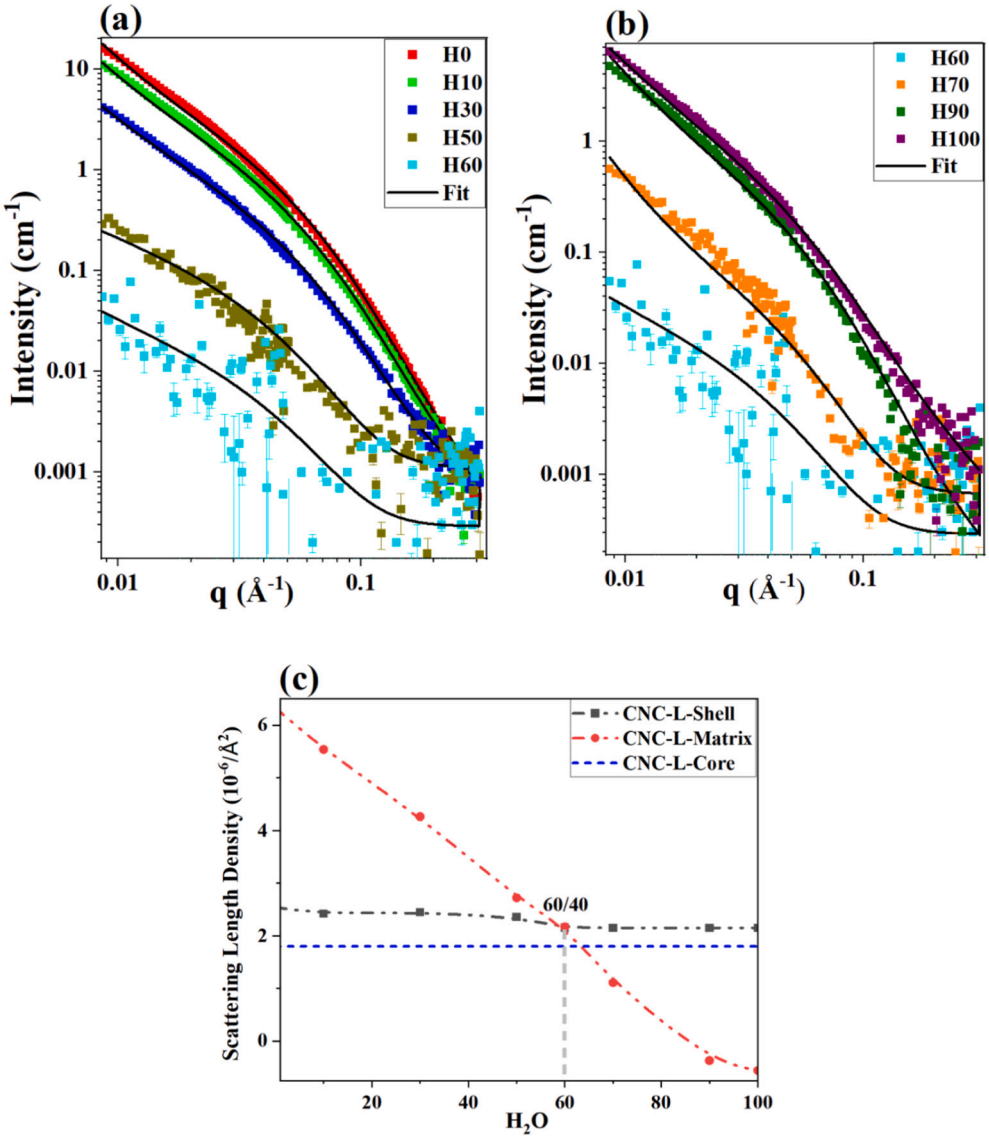

Fig. 2. (a) Intensity-q vector SANS curves from nanocellulose crystal (CNC-**Low**) suspensions measured in H_2O/D_2O at ratios of: (a) H10 to H60 (wt%) and (b) H60 to H100 (wt%). (c) Experimental SLD variation profile of core (pure cellulose), shell and matrix are plotted against H_2O concentration. The contrast matching point for shell and matrix is at 60/40.

3.6. Fourier Transform Infra-red spectroscopy (FTIR)

FTIR measurements were conducted on MCC, CNC-**Low**, CNC-**High** and CNF samples dispersed in H_2O, D_2O and H_2O/D2O at the 60/40 ratio. All samples were air dried overnight at ambient conditions to remove the unexchanged D_2O.

Fig. 5a shows the FTIR spectra of all these air dried samples. All spectra look similar and indicate the characteristic peaks and signals from the cellulose. In cellulose, the broad peak at 3300 cm^{-1} corresponds to the O—H stretching. The peaks at 2900 cm^{-1} represent the stretching vibrations of C—H group in the glucose unit. The peak at 1605 cm^{-1} in CNF is from the COO- group which appears after TEMPO oxidation (Mendoza, Browne, Raghuwanshi, Simon, & Garnier, 2019). The peaks between 1420 and 896 cm^{-1} correspond to the CH_2 symmetric bending, C—O stretching and CH_2 rocking (Chieng, Lee, Ibrahim, Then, & Loo, 2017). The peak at 1640 cm^{-1} appears from the O—H bending vibration. The CNC-**Low** and CNC-**High** show the peak at 810 cm^{-1} which corresponds to the sulfonation where the sulfate half ester groups is linked with the CNC (Espíndola, Pronk, Zlopasa, Picken, & van Loosdrecht, 2021).

However, upon closer analysis of the spectra between 2600 cm^{-1} and 2200 cm^{-1}, there is a clear identification of the -OD peak around 2460 cm^{-1} for the samples MCC-D_2O, MCC-H_2O/D_2O:60/40 and CNC-**Low**-D_2O (Fig. 5b and c) (Raghuwanshi et al., 2017; Su et al., 2016). This -OD peak in the spectra confirms the exchange of H with D in MCC and CNC-**Low**. These results are in agreement with the previous FTIR study on Avicel cellulose studied at different relative humidity (RH) (Driemeier, Mendes, & Ling, 2015). As the RH increases to 60 %, the -OD exchange peak is still present in the curve indicating the presence of -OD at higher RH. Similarly, MCC exposed to ambient H_2O vapours does not reverse most of the previous deuteration.

The CNC-**Low** in the H_2O/D_2O:60/40 suspension does not show the exchange of H with D as seen in the FTIR spectra of CNC-**Low** in H_2O (Fig. 5b).

3.7. Theoretical scattering contrast variation

The theoretical scattering contrast was calculated from the SLD difference of the various types of cellulose with the SLD of the dispersed media at different H_2O/D_2O ratios ranging between 0 and 100. Fig. 6

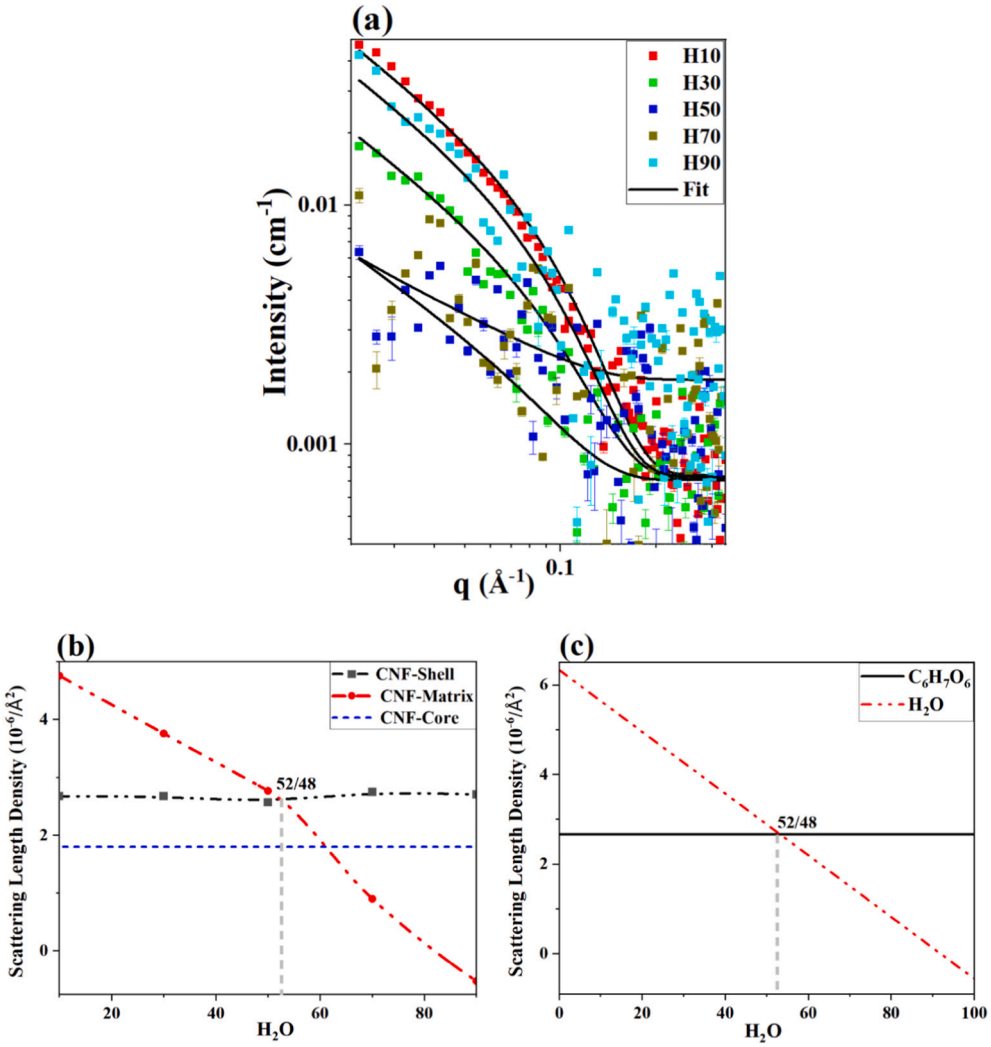

Fig. 3. (a) Intensity- q vector SANS curves from TEMPO oxide nanocellulose fiber (CNF) in H_2O/D_2O at ratios of: (a) H10 to H90 (wt%), (b) Experimental SLD variation profile of core (pure cellulose), shell and matrix are plotted against the H_2O concentration. The contrast matching point for shell and matrix is at 52/48 (c) Theoretical SLD of CNF plotted against D_2O concentration. The cross section at H_2O/D_2O ratio of 52/48 is the contrast matching point.

shows the contrast profile of CNC (with sulfate group), TEMPO-oxidized CNF (with carboxyl group) and MCC (Pure cellulose without any group). Different levels of exchange of H with D on the cellulose monomer unit were considered during the scattering contrast calculations.

The microcrystalline cellulose (MCC) is considered as pure cellulose - without any functional groups. The chemical composition of MCC is $C_6H_{10}O_5$. Without any exchange of H with D, the scattering contrast minimum is calculated at the H_2O/D_2O ratio of 65/35 (Fig. 6a). Exchange of 1H with 1D ($C_6D_1H_9O_5$) shifts the contrast minimum towards lower value at a H_2O/D_2O ratio of 58/42. Exchange of 2H with 2D ($C_6D_2H_8O_5$) shifts further the contrast minimum towards the lower value H_2O/D_2O ratio of 50/50. Replacing all 3H with 3D ($C_6D_3H_7O_5$) moves the scattering contrast minimum towards the lower value at a H_2O/D_2O ratio of 40/60. These results indicate that substitution of OH by functional groups in the cellulose monomeric unit has a significant effect on the scattering contrast matching values.

The TEMPO-oxidized CNF ($C_6H_7O_6$) has carboxylate ($-COO^-$) as functional group. The scattering contrast minima without any exchange of H with D are showed at the H_2O/D_2O ratio of 52/48 (Fig. 6b). Exchange of 1H with 1D ($C_6D_1H_6O_6^-$) shifts the scattering contrast minima towards the lower H_2O/D_2O ratio of 45/55. The further exchange of 2H with 2D ($C_6D_2H_5O_6^-$) further moves the scattering contrast minima towards the lower end of H_2O/D_2O ratio of 38/62.

Fig. 6c shows the scattering contrast for CNC bearing the sulfate group. It is assumed that both CNC-**Low** and CNC-**High** have the same chemical composition with the same functional group ($C_6H_9SO_8^-$). The contract matching point (or minimum) without any exchange of H with D is found at the H_2O/D_2O ratio of 60/40. The exchange of 1H with 1D ($C_6D_1H_8SO_8$) shifts the contrast minimum value towards the lower H_2O/D_2O ratio of 55/45. Further replacing 2H with 2D ($C_6D_2H_7SO_8^-$) further shifts the contrast minima to 50/50.

3.8. CNF contrast matching for PNIPAM-grafted-CNF

Fig. 7 shows the SANS scattering curves of PNIPAM grafted on the CNF (PNIPAM-grafted-CNF) measured at two different temperatures which are below (25 °C) and above (45 °C) the lower critical solution temperatures (LCST) of PNIPAM-grafted-CNF (36 °C). Two different sample of PNIPAM-grafted-CNF were prepared; the first in pure H_2O (PCNF-H100) and the second in H_2O/D_2O at a ratio 60/40 (PCNF-H60). The H100 provides a large contrast for TEMPO-oxidized CNF while H60 is near the contrast matching point of CNF as observed above.

The SANS curve of PNIPAM-grafted-CNF in H100 at 25 °C shows a scattering profile which contains contributions from both PNIPAM and CNF (Fig. 7a). The scattering is mostly dominated by the CNF as seen by the similar scattering from the pure CNF in H_2O. Interestingly, PCNF-

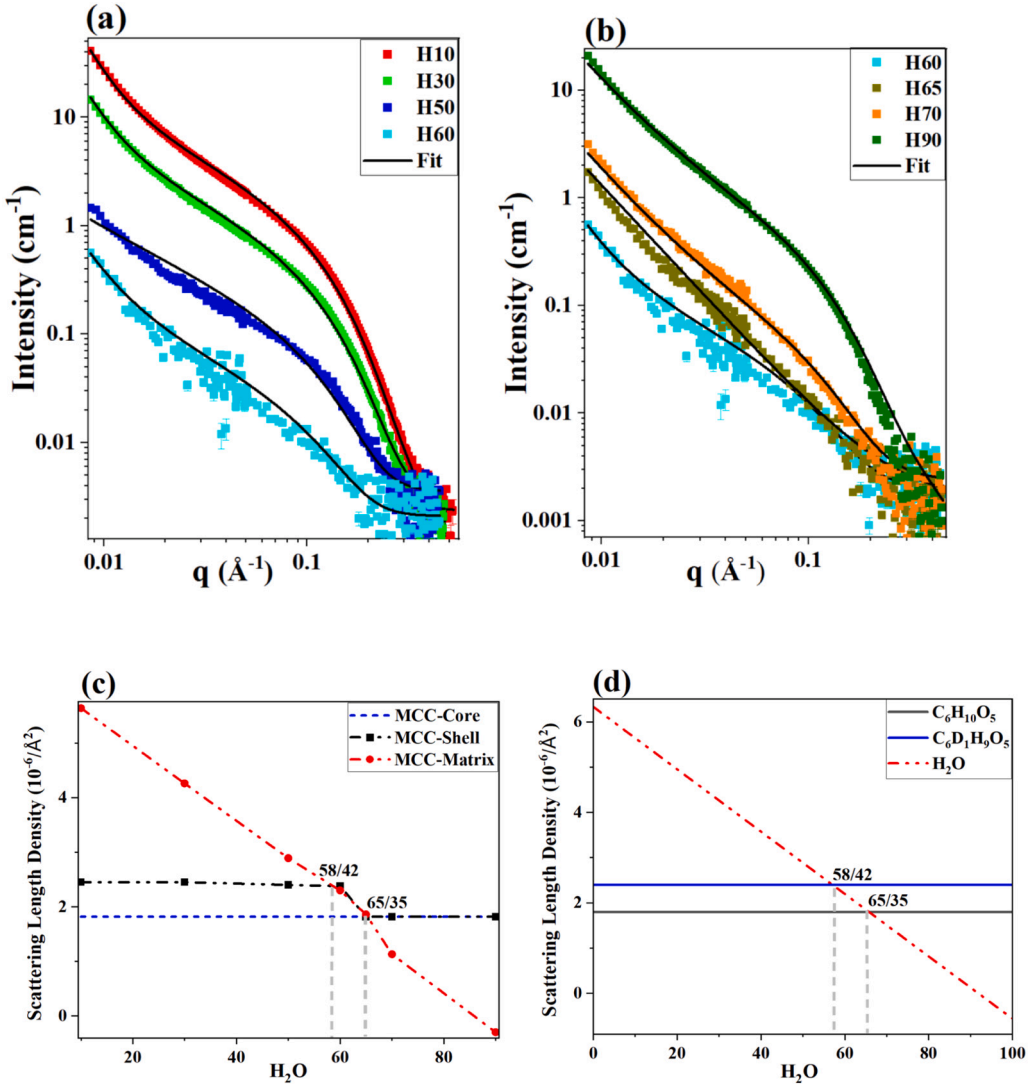

Fig. 4. (a) Intensity-q vector SANS curves from microcrystalline cellulose (MCC) suspensions measured in H_2O/D_2O at ratios of: (a)H10 to H60 (wt%) and (b) H60 to H90 (wt%). (c) Experimental SLD variation profile of core (pure cellulose), shell and matrix are plotted against H2O concentration. The contrast matching point for shell and matrix is at 58/42 (d) Theoretical SLD of MCC without and with exchange of one H with one D with change in D_2O concentration. The cross section at H_2O/D_2O ratio 65/35 for $C_6H_{10}O_5$ and ratio of 58/42 for $C_6D_1H_9O_5$ are the contrast matching points.

H60 eliminates scattering from the CNF, revealing the scattering profile only from the PNIPAM distribution. The scattering profile of pure PNIPAM follows the $q^{-1.3}$ power law which highlights that the scattering originates from the open chain structures of PNIPAM (Gommes, Jaksch, & Frielinghaus, 2021).

Above LCST (at 45 °C), PCNF-H100 shows different SANS scattering profile compared to PCNF below LCST (Fig. 7b). Above LCST, P-CNF-H100 shows an increase in the scattering intensity due to the change of PNIPAM conformation from open chains to closed globules in the network. The scattering profile in Fig. 7b combines scattering contribution from both PNIPAM and CNF. The scattering profile of pure CNF in H100 merges well with the PCNF-H100 scattering profile between the q range 0.03 to 1 Å^{-1}. Near contrast the matching point of the CNF, any scattering contribution from CNF are excluded, revealing exclusively scattering from the PNIPAM distribution in the full system. The PNIPAM scattering follows the q^{-4} power law profile which indicates the presence of large globule structures (Gommes et al., 2021).

4. Discussion

The isotopic exchange of H with D in pure cellulose and functionalized nanocellulose suspensions was studied by SANS at different H_2O/D_2O ratios. The nanocellulose crystals (CNC-**Low** and CNC-**High**) have sulfate groups while TEMPO-oxidized cellulose nanofiber (CNF) contains carboxyl group on the cellulose monomer unit. The microcrystalline cellulose (MCC) is a pure cellulose without any functional groups.

The SANS intensity for all cellulose suspensions first decreases to a minimum and then increase further with increase in the H_2O/D_2O ratio. At the minimum scattering intensity value, the SLD difference between cellulose and the contrast matching H_2O/D_2O ratio suspension is at its smallest. Near the contrast match point the scattering contribution from cellulose therefore disappears.

Only the outer surface of the CNC and CNF is functionalized with the sulfate and carboxyl groups and exposed for isotopic exchange. Thus, a cylindrical core shell model was applied to fit the SANS curves and evaluate the SLD. In this model, the core is made of pure cellulose and the shell consisted of cellulose units which have exchanged the OH at the C_6 position with a sulfate or carboxyl group. The cross section of shell and matrix reveals the contrast match point of the shell region. The cross section of core and matrix indicates the contrast match point of the core region. The average of these match points represents the contrast

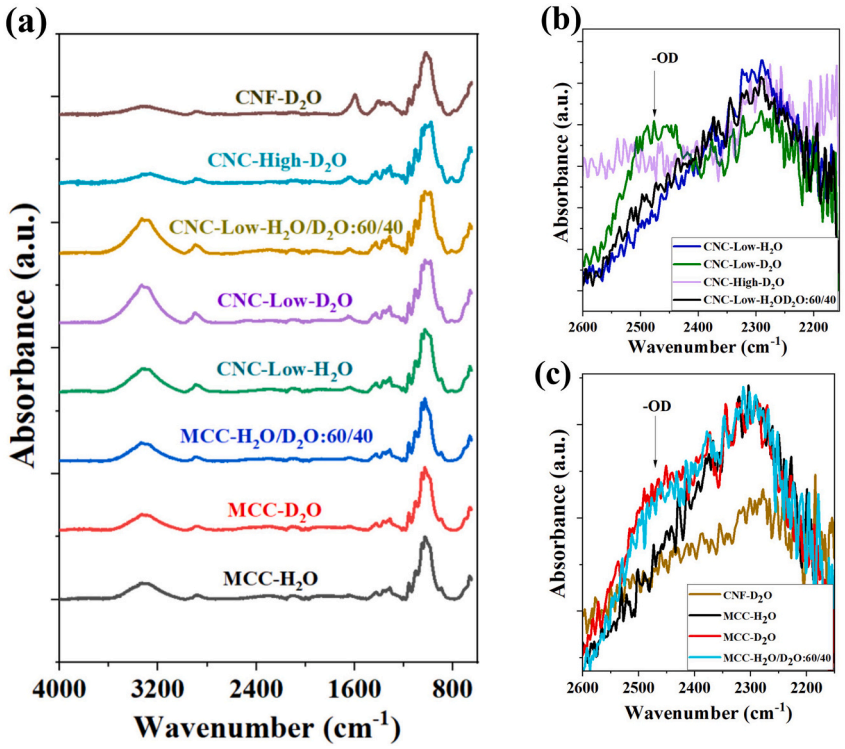

Fig. 5. (a) FTIR spectra of MCC, CNC-**Low**, CNC-**High** and CNF dispersed in H_2O, D_2O and H_2O/D_2O ratio of 60/40. All samples were air dried overnight in the ambient conditions. (b) FTIR spectra of the CNC-**Low**, CNC-**High** in the H_2O, D_2O compared with the CNC-**Low** in H_2O/D_2O ratio of 60/40. (c) FTIR spectra of the CNF, MCC in the D_2O and H_2O, and compared with the MCC in H_2O/D_2O ratio of 60/40.

matching point of the complete functionalized CNC or CNF system.

In CNC-**High** and CNC-**Low,** the contrast matching H_2O/D_2O ratio is 60/40 which shows no isotopic exchange of H with D. The reason for this absence of exchange is that the labile -OH group at the primary C_6 position was already replaced by a sulfate group during the sulfuric acid hydrolysis process. The FTIR spectra of CNC-**Low** in D_2O showed a strong -OD peak which is not observed in CNC-**High** (Fig. 5b). The CNC-**Low** sustains less sulfate groups (0.53 %S) compared to the CNC-**High** (0.73 %S) (Fig. 8a). Thus, in the CNC-**Low,** labile -OH groups at the C_6 position are available for exchange with -OD from D_2O.

CNF shows the contrast match point at the H_2O/D_2O ratio of 52/48 which is similar to the theoretical value of 52/48 (Fig. 3b). This contrast matching reveals that no isotopic replacement between H and D occurred. This is because most of the -OH group at the C_6 position were replaced with COO^- group during TEMPO oxidation (Isogai, Saito, & Fukuzumi, 2011), 35 (Fig. 8). The oxidation process does not change the crystal structure of cellulose, crystalline index or crystal size (Saito et al., 2009; Saito & Isogai, 2004; Saito, Kimura, Nishiyama, & Isogai, 2007). The absence of -OD peak in the FTIR spectra of CNF in D_2O agrees with SANS analysis (Fig. 5c).

MCC shows the contrast matching point at a H_2O/D_2O ratio of 60/40 indicating the exchange of 1H with 1D for a monomer composition of $C_6D_1H_9O_5$ (Fig. 6a). The FITR spectra of MCC in D_2O and 60/40 H_2O/D_2O suspension confirm the -OD peak at 2460 cm^{-1} (Fig. 5b) (Raghuwanshi et al., 2017; Su et al., 2016). Previously, the contrast match point for cellulose microfibrils from wood and Tencel was reported to be at a 65/35 H_2O/D_2O ratio (Crawshaw et al., 2000; Penttilä et al., 2021). The difference in the contrast matching for MCC and wood might be due to the exchange of 1D with the labile 1H linked with C_6 carbon on the monomer unit in MCC. However, for wood and Tencel, the pure cellulose monomer unit is considered where no exchange of D with H occurs. Another reason can be the difference in crystallinity in MCC and wood. Hydroxyl groups are reported to exchange rapidly with D in the amorphous region of cellulose, while the exchange process in the crystalline region is slow (Nakai, FUKUOKA, NAKAJIMA, & HASEGAWA, 1977).

Contrast matching was performed with PNIPAM-grafted-CNF both below and above LSCT and performed near (H_2O/D_2O:60/40) and far (H_2O/D_2O:100/0) from the matching point of CNF. Results show the scattering from CNF was quenched at H_2O/D_2O:60/40 so that only the scattering contribution from PNIPAM was visualized in the scattering curves (Fig. 7a). Below LCST (at 25 °C), the slope of $q^{-1.3}$ for PCNF-60 indicates that the grafted PNIPAM over CNF is a semi-flexible object which is due to grafting (Fig. 7a). The slope of the pure PNIPAM (NIPAM-H100) shows a power law of $q^{-1.6}$ indicating the PNIPAM follows a random coil conformation, with and without self-avoiding interactions (Fig. 7a).

Above LCST (at 45 °C), the PNIPAM chain changes its conformation from an open coil to a globule which follows the q^{-4} power law (Fig. 7b). The slope of q^{-4} indicates the formation of large structures of CNFs bounded with the collapsed grafted polymer, as reported previously (Raghuwanshi, Mendoza, et al., 2023). The schematic of the contrast matching of cellulose is provided in Fig. 8b. The results agree well with the previous findings on the conformational changes in the PNIPAM both below and above the LCST temperature (Katsumoto, Tanaka, Sato, & Ozaki, 2002). For the first time, this study has elucidated the polymer physics challenge of measuring the coil to globule transition of PNIPAM grafted onto CNF.

5. Conclusion

Contrast matching by isotopic exchange of H with D in micro- and nano- cellulose with and without functional groups is studied by SANS and FTIR. A cylindrical core-shell form factor is considered to model the SANS curves and evaluate the SLD of core, shell and matrix. Only the surface is exposed to the functionalisation and isotopic exchange while the inner core remains as pure cellulose. Pure microcrystalline cellulose (MCC) without any functional group showed shell contrast matching at H_2O/D_2O ratio of 58/42 due to the exchange of one -OH with one -OD

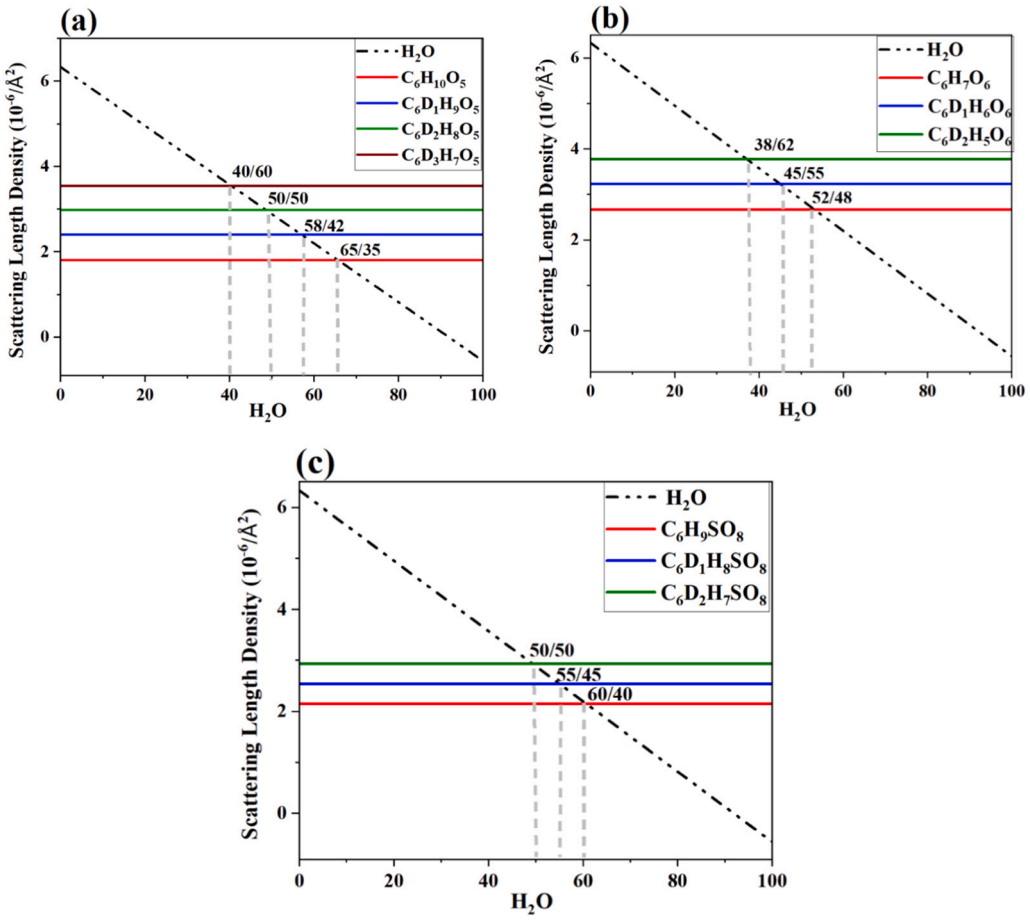

Fig. 6. (a) Theoretical contrast profile calculated for the different types of cellulose varying in chemical composition (functional groups). (a) Pure cellulose - with NO functional groups, (b) cellulose nanofibers (CNF) with COO^- groups and (c) cellulose nanocrystals (CNC) with SO_4^- groups. The contrast is evaluated by considering exchange of different numbers of -OH for -OD groups.

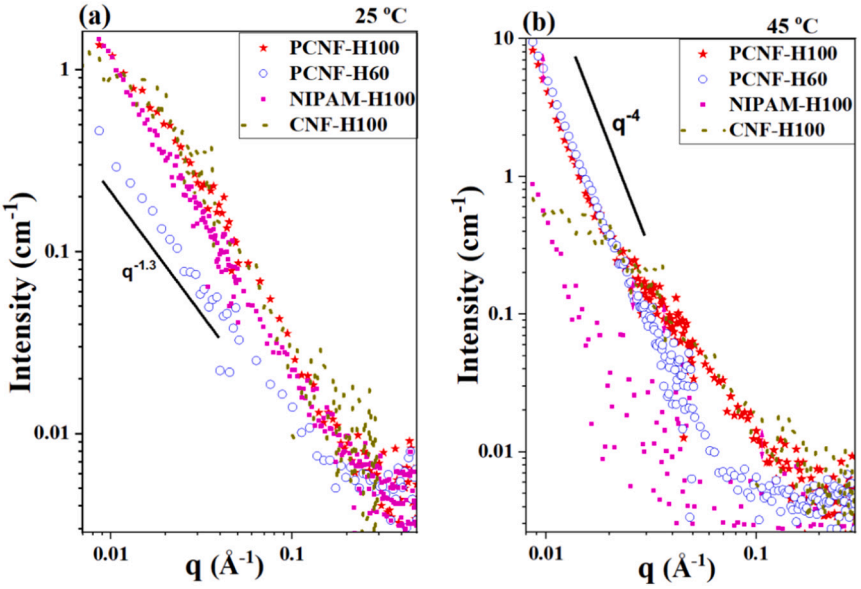

Fig. 7. (a) SANS curves of PNIPAM-grafted-CNF (PCNF-H100) measured in H_2O at 25 °C (below LCST) and near the contrast matching point of CNF (H_2O/D_2O ratio 60/40). SANS curve of PNIPAM in H_2O and CNF in D_2O are included for comparison. (b) SANS curves of PNIPAM-grafted-CNF measured in H_2O at 45 °C (above LCST) and near the contrast matching point of CNF (H_2O/D_2O ratio 60/40). SANS curve of PNIPAM in H_2O and CNF in D_2O are included for comparison.

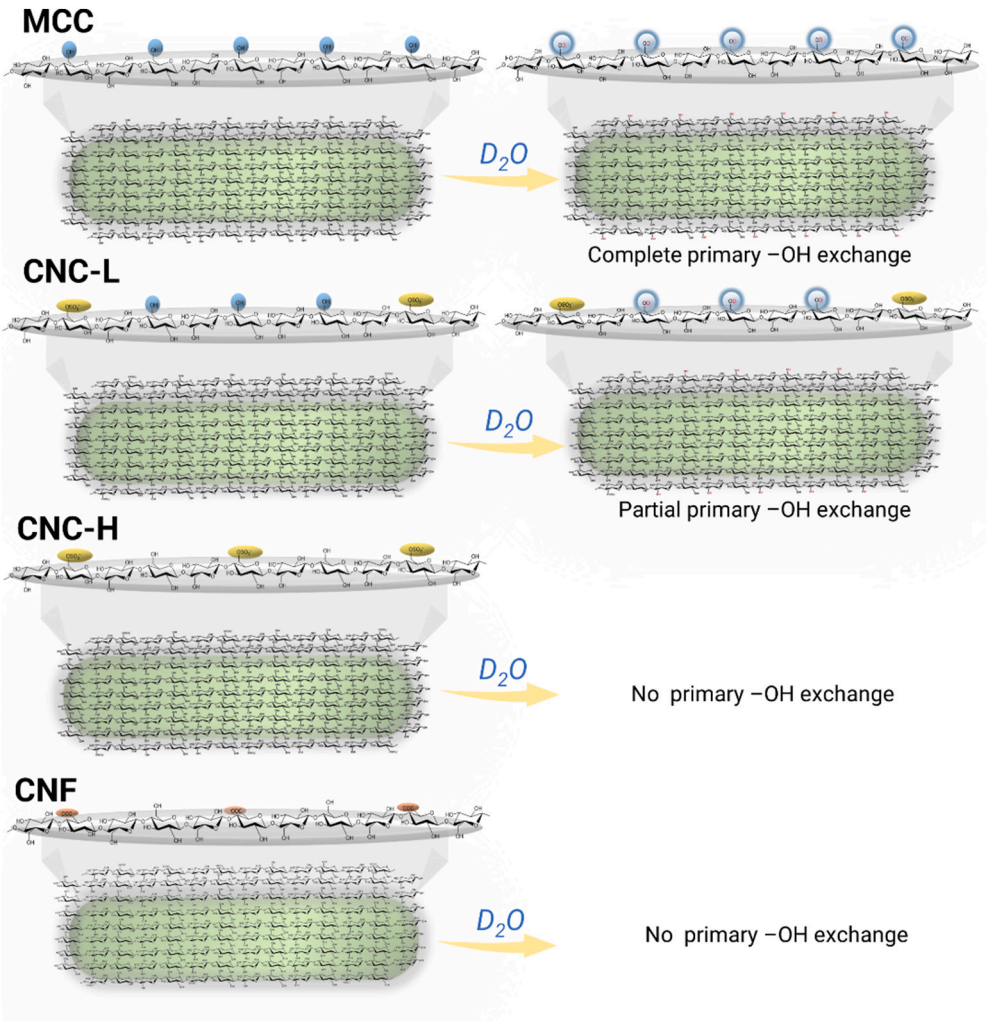

Fig. 8. Schematic representation showing the isotopic exchange of H with D for different nanocellulose (CNC-**Low**, CNC-**High**, CNF) and pure cellulose MCC.

group. For MCC, the labile -OH group linked at the primary C_6 position of the cellulose monomeric unit exchanges easily with the -OD group.

By contrast, the functional nanocellulose CNF surface with -COO^- and CNC surface with -SO_4^- groups showed no exchange of H with D. The contrast matching point for CNC exists at 60/40 and for CNF at 52/48 without any isotopic exchange. The FTIR spectra are in accordance with the SANS results. For TEMPO CNF and acid treated CNC, the functional COO^- and SO_4^- have already replaced the -OH group at the C_6 position during preparation. Thus, no further isotopic exchange occurs in the H_2O/D_2O suspension.

Surprisingly, CNC with a lower sulfur content (CNC-**Low**) dispersed in pure D_2O revealed the exchange of 1H with 1D by FTIR which was not observed for CNC-**High**. In the CNC-**High** all the labile -OH groups at the C_6 positions in the cellulose chains are replaced by the sulfate groups. Thus, no labile -OH groups are available for H to D exchange in CNC-**High**. However, fewer sulfate groups replace the -OH groups at the C_6 positions in the cellulose chains of CNC-**Low**. Thus, the available labile -OH groups at the C_6 position are easily replaced with the D once in pure D_2O environment.

The benefits of cellulose contrast matching are validated by the SANS analysis of the thermosensitive PNIPAM-grafted-CNF hydrogels measured at the high and low contrast matching point of CNF. Contrast matching excluded the scattering contribution from CNF so the distribution of PNIPAM chains below and above LCST could be elucidated by power law variation. Below LCST, the SANS profile of PNIPAM follows the $q^{-1.3}$ power law, revealing its open coil conformation. Above LCST, the PNIPAM scattering contribution follows a q^{-4} power law showing globule formation.

The study shed light on the importance of functional groups contributions in the cellulose glucosidic monomer during isotopic exchange of H with D. Visualization of entities distribution in a nanocellulose network by contrast matching is important to modulate functionality of advanced cellulosic materials in biopharmaceutical, food, and photonics applications.

CRediT authorship contribution statement

Vikram Singh Raghuwanshi: Writing – review & editing, Writing – original draft, Visualization, Validation, Methodology, Investigation, Formal analysis, Data curation, Conceptualization. **David Joram Mendoza:** Writing – review & editing, Writing – original draft, Visualization, Data curation. **Jitendra Mata:** Writing – review & editing, Writing – original draft, Validation, Methodology, Formal analysis, Data curation. **Gil Garnier:** Writing – review & editing, Writing – original draft, Validation, Supervision.

Declaration of competing interest

The authors declare that they have no known competing financial interests or personal relationships that could have appeared to influence the work reported in this paper.

Data availability

Data will be made available on request.

Acknowledgments

We acknowledge funding from the Australian Research Council (ARC) - Industrial Transformation Hub Grant IH130100016. Thanks to the Australian Nuclear Science and Technology Organisation (ANSTO) for the beamtime (Proposal ID: DB 17373). Authors thank to Dr. Christine Browne and Asso/Prof. Warren Batchelor for assistance during beamtime.

Appendix A. Supplementary data

Supplementary data to this article can be found online at https://doi.org/10.1016/j.carbpol.2024.122591.

References

Amoroso, L., De France, K. J., Milz, C. I., Siqueira, G., Zimmermann, T., & Nyström, G. (2022). Sustainable cellulose nanofiber films from carrot pomace as Sprayable coatings for food packaging applications. *ACS Sustainable Chemistry & Engineering, 10*(1), 342–352.

Bethke, K., Palantöken, S., Andrei, V., Roß, M., Raghuwanshi, V. S., Kettemann, F., … Rademann, K. (2018). Functionalized cellulose for water purification, antimicrobial applications, and sensors. *Advanced Functional Materials, 28*(23), Article 1800409.

Breßler, I., Kohlbrecher, J., & Thünemann, A. F. (2015). SASfit: A tool for small-angle scattering data analysis using a library of analytical expressions. *Journal of Applied Crystallography, 48*(Pt 5), 1587–1598.

Browne, C., Raghuwanshi, V. S., Lin, M., Garnier, G., & Batchelor, W. (2022). Characterisation of cellulose nanocrystals by rheology and small angle X-ray scattering (SAXS). *Colloids and Surfaces A: Physicochemical and Engineering Aspects, 651*, Article 129532.

Cheng, G., Liu, Z., Murton, J. K., Jablin, M., Dubey, M., Majewski, J., … Kent, M. S. (2011). Neutron reflectometry and QCM-D study of the interaction of Cellulases with films of amorphous cellulose. *Biomacromolecules, 12*(6), 2216–2224.

Chieng, B. W., Lee, S. H., Ibrahim, N. A., Then, Y. Y., & Loo, Y. Y. (2017). Isolation and characterization of cellulose nanocrystals from oil palm Mesocarp Fiber. *Polymers (Basel), 9*(8).

Crawshaw, J., Vickers, M. E., Briggs, N. P., Heenan, R. K., & Cameron, R. E. (2000). The hydration of TENCEL® cellulose fibres studied using contrast variation in small angle neutron scattering. *Polymer, 41*(5), 1873–1881.

Curvello, R., Raghuwanshi, V. S., & Garnier, G. (2019). Engineering nanocellulose hydrogels for biomedical applications. *Advances in Colloid and Interface Science, 267*, 47–61.

Driemeier, C., Mendes, F. M., & Ling, L. Y. (2015). Hydrated fractions of cellulosics probed by infrared spectroscopy coupled with dynamics of deuterium exchange. *Carbohydrate Polymers, 127*, 152–159.

Espíndola, S. P., Pronk, M., Zlopasa, J., Picken, S. J., & van Loosdrecht, M. C. M. (2021). Nanocellulose recovery from domestic wastewater. *Journal of Cleaner Production, 280*, Article 124507.

Feigin, L. A. S. D. I. (1987). *Structure analysis by small-angle X-ray and Neutron scattering*. New York, NY: Springer.

George, J., & Sabapathi, S. N. (2015). Cellulose nanocrystals: Synthesis, functional properties, and applications. *Nanotechnology, Science and Applications, 8*, 45–54.

Glatter, O. K. O. (1982). *Small angle X-ray scattering: London*. New York: Academic Press.

Gommes, C. J., Jaksch, S., & Frielinghaus, H. (2021). Small-angle scattering for beginners. *Journal of Applied Crystallography, 54*(Pt 6), 1832–1843.

Huang, Z., Raghuwanshi, V. S., & Garnier, G. (2017). Functionality of immunoglobulin G and immunoglobulin M antibody Physisorbed on cellulosic films. *Frontiers in Bioengineering and Biotechnology, 5*, 41.

Isogai, A., Saito, T., & Fukuzumi, H. (2011). *TEMPO-oxidized cellulose nanofibers. Nanoscale, 3*(1), 71–85.

Katsumoto, Y., Tanaka, T., Sato, H., & Ozaki, Y. (2002). Conformational change of poly (N-isopropylacrylamide) during the coil−globule transition investigated by attenuated Total reflection/infrared spectroscopy and density functional theory calculation. *The Journal of Physical Chemistry A, 106*(14), 3429–3435.

Kline, S. R. (2006). Reduction and analysis of SANS and USANS data using IGOR Pro. *Journal of Applied Crystallography, 39*(6), 895–900.

Li, T., Chen, C., Brozena, A. H., Zhu, J. Y., Xu, L., Driemeier, C., … Hu, L. (2021). Developing fibrillated cellulose as a sustainable technological material. *Nature, 590*(7844), 47–56.

Mariano, M., El Kissi, N., & Dufresne, A. (2014). Cellulose nanocrystals and related nanocomposites: Review of some properties and challenges. *Journal of Polymer Science Part B: Polymer Physics, 52*(12), 791–806.

Martínez-Sanz, M., Gidley, M. J., & Gilbert, E. P. (2016). Hierarchical architecture of bacterial cellulose and composite plant cell wall polysaccharide hydrogels using small angle neutron scattering. *Soft Matter, 12*(5), 1534–1549.

Mendoza, D. J., Ayurini, M., Browne, C., Raghuwanshi, V. S., Simon, G. P., Hooper, J. F., & Garnier, G. (2022). Thermoresponsive poly(N-isopropylacrylamide) grafted from cellulose nanofibers via silver-promoted Decarboxylative radical polymerization. *Biomacromolecules, 23*(4), 1610–1621.

Mendoza, D. J., Browne, C., Raghuwanshi, V. S., Simon, G. P., & Garnier, G. (2019). One-shot TEMPO-periodate oxidation of native cellulose. *Carbohydrate Polymers, 226*, Article 115292.

Müller, L. A. E., Zingg, A., Arcifa, A., Zimmermann, T., Nyström, G., Burgert, I., & Siqueira, G. (2022). Functionalized cellulose nanocrystals as active reinforcements for light-actuated 3D-printed structures. *ACS Nano, 16*(11), 18210–18222.

Nakai, Y., Fukuoka, E., Nakajima, S., & Hasegawa, J. (1977). Crystallinity and physical characteristics of microcrystalline cellulose. *Chemical and Pharmaceutical Bulletin, 25*(1), 96–101.

Okita, Y., Saito, T., & Isogai, A. (2010). Entire surface oxidation of various cellulose microfibrils by TEMPO-mediated oxidation. *Biomacromolecules, 11*(6), 1696–1700.

Penttilä, P. A., Zitting, A., Lourençon, T., Altgen, M., Schweins, R., & Rautkari, L. (2021). Water-accessibility of interfibrillar spaces in spruce wood cell walls. *Cellulose, 28*(18), 11231–11245.

Perumal, A. B., Nambiar, R. B., Moses, J. A., & Anandharamakrishnan, C. (2022). Nanocellulose: Recent trends and applications in the food industry. *Food Hydrocolloids, 127*, Article 107484.

Raghuwanshi, V. S., Browne, C., Batchelor, W., & Garnier, G. (2023). Self-assembly of cellulose nanocrystals of different lengths. *Journal of Colloid and Interface Science, 630*, 249–259.

Raghuwanshi, V. S., Cohen, Y., Garnier, G., Garvey, C. J., & Garnier, G. (2021). Deuterated bacterial cellulose dissolution in ionic liquids. *Macromolecules, 54*(14), 6982–6989.

Raghuwanshi, V. S., Cohen, Y., Garnier, G., Garvey, C. J., Russell, R. A., Darwish, T., & Garnier, G. (2018). Cellulose dissolution in ionic liquid: Ion binding revealed by neutron scattering. *Macromolecules, 51*(19), 7649–7655.

Raghuwanshi, V. S., & Garnier, G. (2019). Characterisation of hydrogels: Linking the nano to the microscale. *Advances in Colloid and Interface Science, 274*, Article 102044.

Raghuwanshi, V. S., Mendoza, D. J., Browne, C., Ayurini, M., Gervinskas, G., Hooper, J. F., … Garnier, G. (2023). Effect of temperature on the conformation and functionality of poly(N-isopropylacrylamide) (PNIPAM)-grafted nanocellulose hydrogels. *Journal of Colloid and Interface Science, 652*, 1609–1619.

Raghuwanshi, V. S., Su, J., Garvey, C. J., Holt, S. A., Raverty, W., Tabor, R. F., … Garnier, G. (2017). Bio-deuterated cellulose thin films for enhanced contrast in neutron reflectometry. *Cellulose, 24*(1), 11–20.

Raghuwanshi, V. S., Vir, A. B., Lin, M., & Garnier, G. (2023). From transparent to structural white: Modulating nanoscale self-assembly in silica and nanocellulose composites. *Colloids and Surfaces A: Physicochemical and Engineering Aspects, 675*, Article 131999.

Saito, T., Hirota, M., Tamura, N., Kimura, S., Fukuzumi, H., Heux, L., & Isogai, A. (2009). Individualization of nano-sized plant cellulose fibrils by direct surface carboxylation using TEMPO catalyst under neutral conditions. *Biomacromolecules, 10*(7), 1992–1996.

Saito, T., & Isogai, A. (2004). TEMPO-mediated oxidation of native cellulose. The effect of oxidation conditions on chemical and crystal structures of the water-insoluble fractions. *Biomacromolecules, 5*(5), 1983–1989.

Saito, T., Kimura, S., Nishiyama, Y., & Isogai, A. (2007). Cellulose nanofibers prepared by TEMPO-mediated oxidation of native cellulose. *Biomacromolecules, 8*(8), 2485–2491.

Song, Y., Meng, X., Jiang, W., Evans, B. R., Ben, H., Zhang, Y., … Ragauskas, A. J. (2022). Deuterium incorporation into cellulose: A mini-review of biological and chemical methods. *Cellulose, 29*(8), 4269–4286.

Su, J., Raghuwanshi, V. S., Raverty, W., Garvey, C. J., Holden, P. J., Gillon, M., … Garnier, G. (2016). Smooth deuterated cellulose films for the visualisation of adsorbed bio-macromolecules. *Scientific Reports, 6*(1), 36119.

Tang, J., Sisler, J., Grishkewich, N., & Tam, K. C. (2017). Functionalization of cellulose nanocrystals for advanced applications. *Journal of Colloid and Interface Science, 494*, 397–409.

Wada, M., Okano, T., & Sugiyama, J. (1997). Synchrotron-radiated X-ray and neutron diffraction study of native cellulose. *Cellulose, 4*(3), 221–232.

Wohlert, M., Benselfelt, T., Wågberg, L., Furó, I., Berglund, L. A., & Wohlert, J. (2022). Cellulose and the role of hydrogen bonds: Not in charge of everything. *Cellulose, 29*(1), 1–23.

Wood, K., Mata, J. P., Garvey, C. J., Wu, C.-M., Hamilton, W. A., Abbeywick, P., … Gilbert, E. P. (2018). QUOKKA, the pinhole small-angle neutron scattering instrument at the OPAL Research Reactor, Australia: Design, performance, operation and scientific highlights. *Journal of Applied Crystallography, 51*(2), 294–314.

Xu, T., Du, H., Liu, H., Liu, W., Zhang, X., Si, C., … Zhang, K. (2021). Advanced Nanocellulose-based composites for flexible functional energy storage devices. *Advanced Materials, 33*(48), Article 2101368.

Yano, H., Omura, H., Honma, Y., Okumura, H., Sano, H., & Nakatsubo, F. (2018). Designing cellulose nanofiber surface for high density polyethylene reinforcement. *Cellulose, 25*(6), 3351–3362.